Near-field investigation of spatial variations of $(20\bar{2}\bar{1})$ InGaN quantum well emission spectra

S. Marcinkevičius,[1,a)] Y. Zhao,[2] K. M. Kelchner,[2] S. Nakamura,[2] S. P. DenBaars,[2] and J. S. Speck[2]
[1]*Department of Materials and Nanophysics, KTH Royal Institute of Technology, Electrum 229, 16440 Kista, Sweden*
[2]*Materials Department, University of California, Santa Barbara, California 93106, USA*

(Received 22 July 2013; accepted 15 September 2013; published online 27 September 2013)

Scanning near-field optical spectroscopy was applied to semipolar $(20\bar{2}\bar{1})$ InGaN/GaN quantum wells (QWs) to evaluate spatial homogeneity of QW band gap and its dependence on the growth conditions. In the most uniform QW, photoluminescence (PL) spectra were found to be narrow with small peak wavelength and spectral width variations. A QW grown at reduced temperature showed sub-micrometer size PL features aligned along the **a** axis and caused by nonuniform In incorporation at surface undulations. At extended defects, complex and strongly varying near-field spectra were observed and tentatively assigned to QW segments of different orientations around these defects. © *2013 AIP Publishing LLC*. [http://dx.doi.org/10.1063/1.4823589]

Semipolar $(20\bar{2}\bar{1})$ InGaN/GaN quantum wells (QWs) have recently emerged as an alternative to QWs grown on polar *c* and nonpolar *a* and *m* planes for fabrication of light emitting diodes (LEDs) and lasers.[1] Compared to the polar structures, the semipolar ones experience smaller intrinsic electric fields, caused by the difference in spontaneous and piezoelectric polarizations in the barrier and well layers.[2] The advantage of $(20\bar{2}\bar{1})$ over nonpolar InGaN QWs is a more effective In incorporation under the same growth conditions,[3] leading to longer emission wavelengths including those in the green[4] and yellow-green[5] spectral regions. Besides, semipolar QWs show narrower widths of the emission spectra, which is advantageous for laser applications. However, the spectral linewidths are sample dependent and strongly increase with the emission wavelength, indicating that carrier localization occurs in these structures as well. For instance, for $(20\bar{2}\bar{1})$ QWs at room temperature, full width at half maximum (FWHM) values increase from 20 nm in the blue[6,7] to 60 nm in the green-yellow[5] spectral regions. For laser diodes, material gain presumably is inversely proportional to the luminescence linewidth.

So far, emission from $(20\bar{2}\bar{1})$ InGaN QWs has been studied by standard far-field electroluminescence and photoluminescence (PL) techniques. While such data allow rough comparisons of the emission properties of QWs grown on different crystallographic planes and under different conditions, understanding of fine effects, such as influence of structural domains on band potential fluctuations,[8] band gap variations around dislocations,[9] spatial variations of band bending at heterostructures,[10] and formation of hot spots in devices,[11] requires information on spatial distribution of the emission spectra and their parameters. Confirmation of spatial homogeneity of the emission spectrum requires nanoscale measurement techniques as well. In this work, by applying scanning near-field optical microscopy (SNOM) on a number of semipolar $(20\bar{2}\bar{1})$ InGaN QW structures, we observe dependence of the QW homogeneity on the growth conditions and reveal marked spectral changes occurring around extended defects. The details help identify the optimal conditions for the $(20\bar{2}1)$ QW growth.

The studied structures were grown by metal organic chemical vapor deposition on low defect density bulk $(20\bar{2}\bar{1})$ plane GaN substrates, provided by Mitsubishi Chemical Corporation. The structures consisted of a 1 μm undoped GaN template layer, an InGaN single QW, and a thin 10 nm GaN cap layer. The small thickness of the cap layer was chosen to maintain a good near-field coupling between the probe and the studied QW. Measurements on a QW embedded in a LED *p-i-n* structure with 50 nm thick *p*-side layers produced similar data showing that a longer thermal exposure of the QW during growth of a thicker cap layer does not affect the band potential uniformity of the QW. To reduce the influence of the built-in electric field on the emission properties, narrow 3 nm wide QWs were used. The growth temperature for structures A, B, and C was 840, 850, and 855 °C, and In percentage in the QW was estimated as 27%, 25%, and 24%, respectively.

Near-field PL scans were performed at room temperature with a SNOM apparatus operating in the illumination-collection mode. Aluminum-coated UV fiber probes with 100 nm aperture diameter were used. PL was excited directly into the QW by 200 fs frequency doubled Ti:sapphire laser pulses with a 375 nm central wavelength. The photoexcited carrier density, evaluated from the average excitation power density, probe throughput, aperture diameter, and InGaN absorption coefficient was below 5×10^{11} cm^{-2}. For PL detection, a spectrometer equipped with a liquid nitrogen cooled charge coupled device detector was employed. Scanned areas varied from 4×4 to 10×10 μm^2 with scanning steps between 50 and 100 nm. Full PL spectrum was recorded at each point of a scan. Due to the multimode character of the optical fiber, PL polarization was not resolved. Spatial resolution of the measurements was limited by the probe aperture diameter.

a)Electronic mail: sm@kth.se

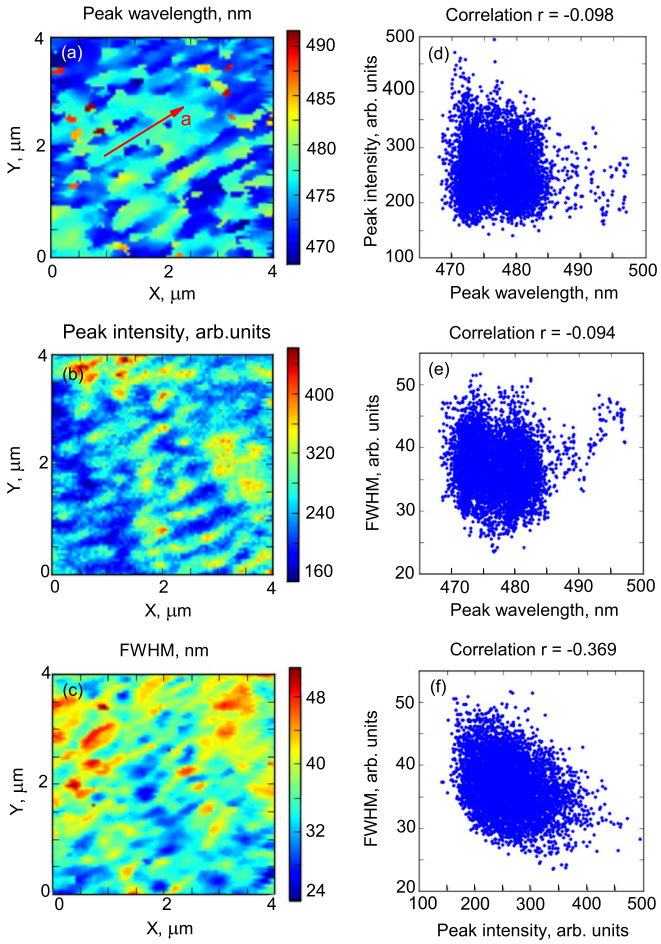

FIG. 1. Near-field PL maps of peak wavelength (a), peak intensity (b), and FWHM (c), as well as correlation graphs between peak intensity and peak wavelength (d), FWHM and peak wavelength (e), and FWHM and peak intensity (f) for sample A.

Figure 1 shows maps of the peak wavelength, peak intensity, and FWHM generated from the near-field PL spectra of sample A. Along with the maps, correlation graphs between peak wavelength, peak intensity, and FWHM are displayed. One can notice that the maps are composed of sub-μm size features aligned along the **a** axis, and the span of parameter variation is quite large. The correlations between the peak intensity and wavelength and the FWHM and wavelength are almost absent, with most of the spectra having the peak wavelength and peak intensity in the middle of the scale. Only the FWHM–intensity correlation shows a notable negative trend, with narrower peaks tending to be more intense. The Pearson product-moment correlation coefficient for this correlation is $r = -0.369$.

The near-field maps for samples B and C, however, are quite different. Fig. 2 shows peak wavelength and FWHM maps measured for sample B. Maps from other scans performed on samples B and C show qualitatively similar features. For these samples, the span of spectral parameter variation is much smaller, the islands of close values are much larger, and the map features have no preferential direction. The correlations for different scans between the peak wavelength and intensity, as well as the peak wavelength and FWHM fluctuate between small negative and positive values; only the peak intensity–FWHM correlation, similarly as for sample A, is clearly negative.

The average values and deviations for the measured data are gathered in Table I. One can notice that the peak wavelength deviation, which is relatively large for sample A, can be as small as 0.9 nm (sample C). The ratio of the peak intensity deviation and its value for various scans is only 0.1 for the samples grown at higher temperatures. FWHM deviation may reach as little as 1 nm with the smallest FWHM value falling below 20 nm. This is quite remarkable for QWs emitting at around 480 nm, especially when compared to typical FWHM values of ~50 nm for nonpolar QWs.[12,13]

The larger FWHM and statistical deviations for sample A stem from more complex near-field spectra, which display a multi-peak structure and experience large point to point variations. In Fig. 3, a typical near-field spectrum of sample A is compared to that of B. In the sample A spectrum, one can notice up to four different components. Since the probed area is 100 nm in diameter, the multi-peak structure indicates that areas with uniform potentials are smaller than that. The near-field spectra for the samples B and C are much more uniform. Still, the spectra are considerably broader than the homogeneous broadening (47 meV or 8.5 nm (Ref. 14)), which shows that even for the most homogeneous samples the nanoscale band potential variations play an important role. Interestingly, the low temperature far-field spectra (not shown) for samples A, B, and C are not that different with the FWHM between 15.5 nm, 92 meV (sample C) and 18 nm, 110 meV (sample A). With increased temperature, the spectra primarily broaden for sample A because of the thermally activated carrier diffusion into lower potential areas, similarly as in nonpolar InGaN QW.[14] For the samples with

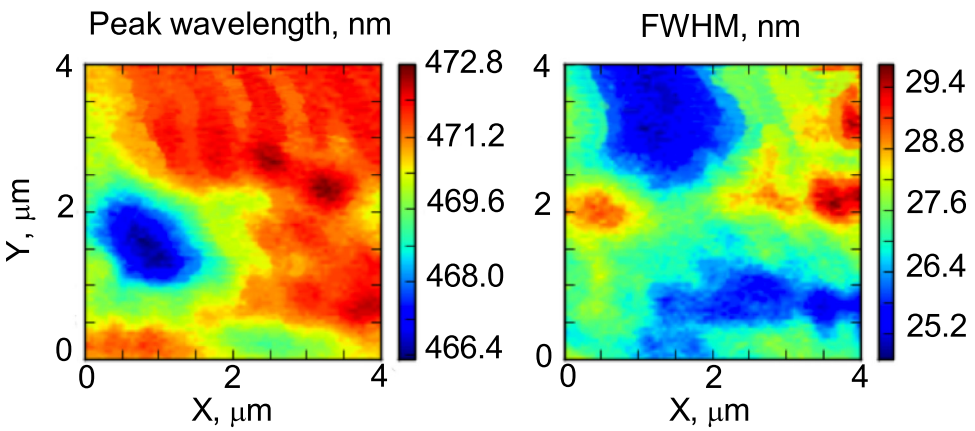

FIG. 2. Near-field PL maps of peak wavelength and FWHM for sample B.

TABLE I. Statistical parameters of the near-field PL scans.

Sample	A	B	C
Peak wavelength, average (nm)	477.4	470.7	457.8
Peak wavelength, deviation (nm)	4.7	1.2	0.8
Peak intensity deviation/average	0.16	0.10	0.11
Average FWHM, nm (meV)	36.2 (197)	27.2 (151)	23.7 (140)
FWHM deviation, nm (meV)	4.2 (23)	1.0 (6)	1.7 (10)
Localization parameter σ_L (meV)	66	46	41

smaller band potential variations, the temperature-induced broadening is weaker.

The nanoscale band potential variation, manifesting through the broadening of the near-field spectra, can be analysed using a model,[15] in which the depth of the localization centers is assumed to have a Gaussian distribution. The inhomogeneous broadening under the probe aperture is described by a Gaussian joint density of states

$$g_G(E) = \int_{-\infty}^{+\infty} \frac{1}{\sqrt{2\pi\sigma_L}} \exp\left(\frac{{E_1}^2}{2{\sigma_L}^2}\right) g_0(E - E_1) dE_1, \quad (1)$$

where $g_0(E)$ is the density of states of an ideal QW and σ_L is the localization depth parameter, which describes the fine spread of the band gap values and, indirectly, of the composition fluctuations. For low excitation, free carrier and exciton distributions obey Boltzmann statistics; hence, the PL intensity is proportional to $I_{PL}(E) \propto g_G(E)\exp(-E/k_BT)$. The FWHM has contributions from the inhomogeneous Γ_{ih} and the homogeneous broadening, the latter caused by the carrier-phonon interaction[15]

$$\Gamma(T) = \Gamma_{ih} + \beta T + \frac{\gamma}{\exp(\hbar\omega_{LO}/K_BT) - 1}. \quad (2)$$

Here, β and γ represent the carrier/exciton coupling strength with acoustic and LO phonons, respectively. The values of $\hbar\omega_{LO} = 88$ meV, $\beta = 0.035$ meV/K, and $\gamma = 0.75$ eV were taken from the measurements on *m*-plane InGaN QWs of similar composition.[14] Using the experimental data of the FWHM, the localization parameter for different samples is between 41 and 66 meV (Table I).

The difference in the near-field maps, spectra, and localization potentials for sample A, grown at 840 °C and the other ones is quite remarkable. The most probable cause of the well band gap variation is nonuniformity of In distribution, since monolayer-thick well width variations in InGaN QWs would hardly provide large uniform islands, and strain fluctuations in thin 3 nm single QWs grown on homoepitaxial substrates are unlikely. Growth condition-dependent surface undulations along the **a** axis, along which our SNOM features appear, have been observed in $(20\bar{2}\bar{1})$ InGaN QW structures[16] and $(20\bar{2}1)$ InGaN epitaxial layers.[17] In $(20\bar{2}1)$ QWs, surface morphology variations were found to correlate with spatial differences of PL properties.[18] Our experiments show that structural features may affect PL in $(20\bar{2}\bar{1})$ QWs as well. Here, one should note that similarity of physical properties of $(20\bar{2}\bar{1})$ and $(20\bar{2}1)$ is not trivial; for instance, degree of polarization of the emitted radiation, presumably, due to different cation interdiffusions, is largely different.[19]

Morphology features that appear during growth of $(20\bar{2}\bar{1})$ QWs may be related to variations in alloy band gap determined by the nonuniform In incorporation. Different microfacet planes, such as $(10\bar{1}1)$ and $(10\bar{1}0)$, present at undulations,[17] anisotropic material growth at nonpolar planes,[20] and dependence of In incorporation on the crystallographic orientation[3,21] may contribute to the SNOM map features of sample A. At higher growth temperatures, In atoms must be overcoming the diffusion barriers related to the undulations and form extended μm-size islands of uniform alloy composition.

The smooth QW potentials with spatially uniform alloy composition become very different around defects. Fig. 4 shows a scan for sample C in which very strong local variations in the spectral parameters and multi-structured near-field PL spectra are observed. The peak wavelength map shows that the short wavelength component is dominating the spectra within areas of one to two hundred nm in diameter; however, the FWHM map indicates that the broadened

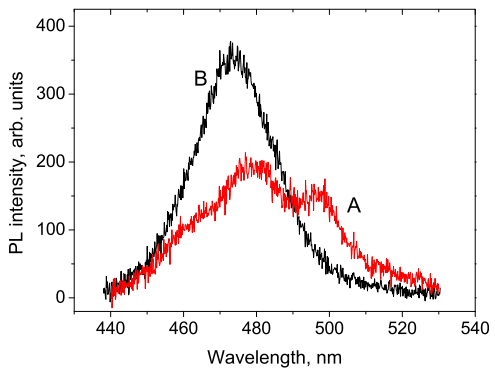

FIG. 3. Typical near-field PL spectra of samples A and B.

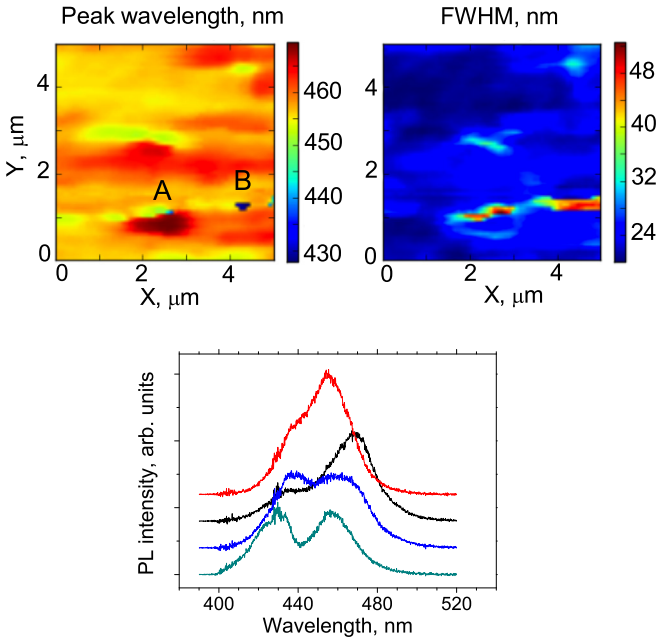

FIG. 4. Peak wavelength (a) and FWHM (b) maps measured in the vicinity of an area containing defects. Near-field spectra around the defect A (c) have large wavelength and shape variations.

spectra with both, long and short wavelength components, extend over larger regions. Besides, as Fig. 4(c) shows, peak wavelengths and intensity in the double peak structure vary with position.

The spatial variations of the PL spectra imply a large variation of In content around the defects or variation of the well width. Previously, dual wavelength emission was observed in *c*-plane InGaN QWs around V-shaped defects.[22] The short wavelength peak was attributed to the narrower QW width and the smaller piezoelectric field in the QW segments located at the extended V-shaped pits. SNOM measurements showed that characteristic dimensions of the areas emitting at short wavelengths were about 0.5 to 1 μm, and that the main QW emission was spectrally uniform.[9] Emission at different wavelengths was also observed from QWs grown on different facets of pyramidal GaN mesas[23] and GaN stripes of nonpolar and semipolar orientation.[24] These features were attributed to well width and alloy composition dependence on the symmetry on the QW growth planes.

Segments of different orientations in InGaN QWs may occur not only in V-shape but also in void defects. Such defects, containing $\{000\bar{1}\}$ facets and $\{000\bar{1}\}$ base, were observed in *c*-plane GaN and InGaN.[25] Faceted void defects were also detected in high defect density semipolar InGaN QWs.[16] Thus, it is likely that the dual wavelength emission shown in Fig. 4 originates from areas containing QW segments of different orientations. Strong PL wavelength variations, not only for the short but also for the long wavelength peak (e.g., around defect A, Fig. 4(a)), support this assignment. The PL excitation directly into the QW and the strong localization of the emission containing the short wavelength peak allows excluding such mechanisms as emission from excited QW states and impurity-related transitions in the barriers. For a definite answer about the origin of this effect, near-field investigations with a resolution much higher than 100 nm are necessary. One should note that out of the several tens of thousands spectra, measured during the near-field scans, these features have been observed in less than 10 measurement points, thus, the complicated emission spectra around defects do not affect the spatially integrated far-field emission.

In conclusion, scanning near-field optical spectroscopy has been applied to MOCVD-grown semipolar $(20\bar{2}\bar{1})$ InGaN QWs in order to obtain nanoscale information on band potential variations and their dependence on the growth conditions. In the most uniform QWs, the variations of the emission spectra were found to be small with the peak wavelength and FWHM variations (standard deviation) of about 1 nm. A QW grown at a lower temperature shows features in PL peak wavelength, intensity, and FWHM that are aligned along the **a** axis. These features were attributed to nonuniform In incorporation at surface undulations. At extended defects, complex and strongly varying near-field spectra were observed and tentatively assigned to QW segments of different orientations around these defects.

Research at KTH was performed within the frame of Linnaeus Excellence Center for Advanced Optics and Photonics (ADOPT) and was financially supported by the Swedish Energy Agency (Contract No. 36652-1) and Knut and Alice Wallenberg Foundation. Research at UCSB was supported by the Solid State Lighting and Energy Center (SSLEC).

[1]D. F. Feezell, J. S. Speck, S. P. DenBaars, and S. Nakamura, J. Disp. Technol. **9**, 190 (2013).
[2]R. M. Farrell, E. C. Young, F. Wu, S. P. DenBaars, and J. S. Speck, Semicond. Sci. Technol. **27**, 024001 (2012).
[3]J. E. Northrup, Appl. Phys. Lett. **95**, 133107 (2009).
[4]Y. Zhao, S. H. Oh, F. Wu, Y. Kawaguchi, S. Tanaka, K. Fujito, J. S. Speck, S. P. DenBaars, and S. Nakamura, Appl. Phys. Express **6**, 062102 (2013).
[5]S. Yamamoto, Y. Zhao, C. C. Pan, R. B. Chung, K. Fujito, J. Sonoda, S. P. DenBaars, and S. Nakamura, Appl. Phys. Express **3**, 122102 (2010).
[6]G. A. Garrett, H. Shen, M. Wraback, A. Tyagi, M. C. Schmidt, J. S. Speck, S. P. DenBaars, and S. Nakamura, Phys. Status Solidi C **6**, S800 (2009).
[7]Y. Zhao, S. Tanaka, C. C. Pan, K. Fujito, D. Feezell, J. S. Speck, S. P. DenBaars, and S. Nakamura, Appl. Phys. Express **4**, 082104 (2011).
[8]A. Pinos, V. Liuolia, S. Marcinkevičius, J. Yang, R. Gaska, and M. S. Shur, J. Appl. Phys. **109**, 113516 (2011).
[9]F. Hitzel, G. Klewer, S. Lahmann, U. Rossow, and A. Hangleiter, Phys. Rev. B **72**, 081309R (2005).
[10]V. Liuolia, S. Marcinkevičius, D. Billingsley, M. Shatalov, J. Yang, R. Gaska, and M. S. Shur, Appl. Phys. Lett. **100**, 242104 (2012).
[11]A. Pinos, S. Marcinkevičius, J. Yang, Y. Bilenko, M. Shatalov, R. Gaska, and M. S. Shur, Appl. Phys. Lett. **95**, 181914 (2009).
[12]C. H. Chiu, S. Y. Kuo, M. H. Lo, C. C. Ke, T. C. Wang, Y. T. Lee, H. C. Kuo, T. C. Lu, and S. C. Wang, J. Appl. Phys. **105**, 063105 (2009).
[13]S. Marcinkevičius, K. M. Kelchner, S. Nakamura, S. P. DenBaars, and J. S. Speck, Appl. Phys. Lett. **102**, 101102 (2013).
[14]V. Liuolia, A. Pinos, S. Marcinkevičius, Y. D. Lin, H. Ohta, S. P. DenBaars, and S. Nakamura, Appl. Phys. Lett. **97**, 151106 (2010).
[15]P. G. Eliseev, P. Perlin, J. Lee, and M. Osinski, Appl. Phys. Lett. **71**, 569 (1997).
[16]Y. Zhao, F. Wu, C. Y. Huang, Y. Kawaguchi, S. Tanaka, K. Fujito, J. S. Speck, S. P. DenBaars, and S. Nakamura, Appl. Phys. Lett. **102**, 091905 (2013).
[17]S. Ploch, T. Wernicke, J. Thalmair, M. Lohr, M. Pristovsek, J. Zweck, M. Weyers, and M. Kneissl, J. Cryst. Growth **356**, 70 (2012).
[18]A. Kaneta, Y.-S. Kim, M. Funato, Y. Kawakami, Y. Enya, T. Kyono, M. Ueno, and T. Nakamura, Appl. Phys. Express **5**, 102104 (2012).
[19]Y. Zhao, S. Tanaka, Q. Yan, C.-Y. Huang, R. B. Chung, C.-C. Pan, K. Fujito, D. Feezell, C. G. Van de Walle, J. S. Speck, S. P. DenBaars, and S. Nakamura, Appl. Phys. Lett. **99**, 051109 (2011).
[20]L. Lymperakis and J. Neugebauer, Phys. Rev. B **79**, 241308R (2009).
[21]M. V. Durnev, A. V. Omelchenko, E. V. Yakovlev, I. Yu. Evstratov, and S. Yu. Karpov, Appl. Phys. Lett. **97**, 051904 (2010).
[22]C. Netzel, H. Bremers, L. Hoffmann, D. Fuhrmann, U. Rossow, and A. Hangleiter, Phys. Rev. B **76**, 155322 (2007).
[23]S. Khatsevich, D. H. Rich, X. Zhang, W. Zhou, and P. D. Dapkus, J. Appl. Phys. **95**, 1832 (2004).
[24]B. Neubert, P. Brückner, F. Habel, F. Scholz, T. Riemann, J. Christen, M. Beer, and J. Zweck, Appl. Phys. Lett. **87**, 182111 (2005).
[25]A. B. Yankovich, A. V. Kvit, X. Li, F. Zhang, V. Avrutin, H. Y. Liu, N. Izyumskaya, Ü. Özgür, H. Morkoç, and P. M. Voyles, J. Appl. Phys. **111**, 023517 (2012).